CHIN. PHYS. LETT. Vol. 36, No. 5 (2019) 057302

Anisotropic Transport on Monolayer and Multilayer Phosphorene in the Presence of an Electric Field *

Gufeng Fu(付谷风), Fang Cheng(程芳)**

Department of Physics and Electronic Science, Changsha University of Science and Technology, Changsha 410004

(Received 15 January 2019)

We demonstrate theoretically the anisotropic quantum transport of electrons through an electric field on monolayer and multilayer phosphorene. Using the long-wavelength Hamiltonian with continuum approximation, we find that the transmission probability for transport through an electric field is an oscillating function of incident angle, electric field intensity, as well as the incident energy of electrons. By tuning the electric field intensity and incident angle, the channels can be transited from opaque to transparent. The conductance through the quantum waveguides depends sensitively on the transport direction because of the anisotropic effective mass, and the anisotropy of the conductance can be tuned by the electric field intensity and the number of layers. These behaviors provide us an efficient way to control the transport of phosphorene-based microstructures.

PACS: 73.63.−b, 72.10.−d, 68.65.−k DOI: 10.1088/0256-307X/36/5/057302

Graphene is a popular material found previously owing to its good carrier mobilities and high on/off ratio,[1,2] but its bandgap opening is still one of the largest challenges. Black phosphorus (BP) has a good carrier mobility and possesses a direct band gap 0.3 eV located at the Γ point,[3] and each phosphorus atom is covalently bonded with three adjacent phosphorus atoms to form a puckered honeycomb structure inside a single layer.[4−7] In the last few years, many researchers have turned their attention to black phosphorus due to its unique electronic properties and broad applications in nanoelectronics.[8−16] Black phosphorus is an appealing candidate for tunable photodetection from the visible to the infrared part of the spectrum.[17] The mid-infrared photodetectors based on black arsenic phosphorus have a high detectivity at room temperature.[18] In addition, the field-effect-transistor (FET) based on few-layer BP is found to have an on/off ratio of 10^5 and a carrier mobility at room temperature as high as $10^3\,\mathrm{cm}^2/\mathrm{V}$,[19,20] which makes BP a favorable material for next generation electronic devices.

The anisotropy is a significant feature of BP, which is embodied in optical, magnetic, mechanical and electrical properties of BP.[21−26] Applying an in-plane electric field perpendicular to the nanoribbon direction can control the quasi-flat bands of phosphorene nanoribbons,[27] and can modify the bandgap of BP.[28] The interband and inter-subband transitions in BP can be continuously varied over a wide electromagnetic spectral range from visible to far IR by varying the electric field.[29] In this work, we explore the anisotropic behaviors of electrons through an external perpendicular electric field E_z on monolayer and multilayer BP along the Γ–X and Γ–Y directions. We find that the transmission probability for transport through an external perpendicular electric field is an oscillating function of incident angle, electric field intensity, as well as the incident energy of electrons. The tunneling is forbidden when the incident angle exceeds a critical value. The incident angle for transport along the Γ–X direction $\theta_{0\mathrm{c}}^{(x)}$ is still always $\pi/2$, while the incident angle for transport along the Γ–Y direction $\theta_{0\mathrm{c}}^{(y)}$ is determined by the electric field intensity and the number of layers. Interestingly, because of the anisotropic effective mass, the conductance shows strong anisotropic behavior.

The N-layer problem can be translated into N effective monolayer problems in the long wavelength approximation. The long-wavelength Hamiltonian with continuum approximation for the N-layer BP based on the ten-hopping description for low-energy contribution H is given as[28]

$$H = \begin{pmatrix} H_{11} & H_{12} \\ H_{21} & H_{22} \end{pmatrix}, \tag{1}$$

where $H_{11} = u_0^n + \eta_x^n k_x^2 + \eta_y^n k_y^2$, $H_{12} = \delta^n + \gamma_x^n k_x^2 + \gamma_y^n k_y^2 + i\chi^n k_x$, $H_{21} = \delta^n + \gamma_x^n k_x^2 + \gamma_y^n k_y^2 - i\chi^n k_x$, $H_{22} = u_0^n + \eta_x^n k_x^2 + \eta_y^n k_y^2$, and the parameters are layer-dependent.[28] The low energy physics of N-layer BP around Γ point can be well described by an anisotropic two band $\boldsymbol{k}\cdot\pm p$ model[30]

$$H = \begin{pmatrix} E_\mathrm{c} + \alpha k_x^2 + \beta k_y^2 & \gamma k_x \\ \gamma k_x & E_\mathrm{v} - \lambda k_x^2 - \eta k_y^2 \end{pmatrix}, \tag{2}$$

where $E_\mathrm{c} = u_0^n + \delta^n$ is the conduction band edge, $E_\mathrm{v} = u_0^n - \delta^n$ is the valence band edge, $\alpha = \eta_y^n + \gamma_y^n$, $\beta = \eta_x^n + \gamma_x^n$, $\lambda = \eta_y^n - \gamma_y^n$, $\eta = \eta_x^n - \gamma_x^n$, and $\gamma = \chi^n$. We consider the N-layer BP with an external electric field perpendicular to the surface (see Fig. 1), and the low energy physics of the N-layer BP around Γ point can be well expressed by

$$H = \begin{pmatrix} H_{311} & \gamma k_x \\ \gamma k_x & H_{322} \end{pmatrix}, \tag{3}$$

where $H_{311} = E_\mathrm{c} - V_z + \alpha k_x^2 + \beta k_y^2$, $H_{322} = E_\mathrm{v} + V_z - \lambda k_x^2 - \eta k_y^2$, $V_z = eE_z z$ is the bias potential, z is

*Supported by the National Natural Science Foundation of China under Grant No 11374002, the Scientific Research Fund of Hunan Provincial Education Department under Grant No 17A001, and the Hunan Provincial Key Laboratory of Flexible Electronic Materials Genome Engineering of Changsha University of Science and Technology.

**Corresponding author. Email: chengfang@csust.edu.cn

© 2019 Chinese Physical Society and IOP Publishing Ltd

the thickness of the N-layer BP, and e is the electron charge.

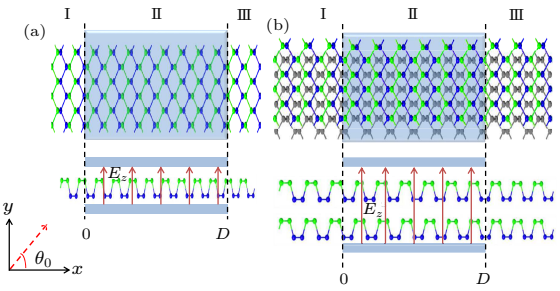

Fig. 1. Schematic of an external perpendicular electric field geometry on the BP. (a) Top and side views of monolayer BP. (b) Top and side views of bilayer BP. Green (blue) balls represent phosphorus atoms in the upper (lower) layer. The shaded regions and the arrowhead regions denote the regions under the electric field. The red dashed arrow represents incident wavevector with angle θ_0. The width of the electric field region is $D = 100$ nm.

We take the transport along the Γ–X direction as an example to explain the calculation method. For electron tunneling through an electric field region in monolayer BP, with $E_z = 0$ in region I ($x < 0$), region III ($x > D$) and $E_z = E_z$ in region II ($0 < x < D$) as shown in Fig. 1, the translational invariance along the y direction gives rise to the conservation of k_y, and thus the solutions to Eq. (3) in the jth region can be written as $\Psi_j(x, y) = \Psi_j(x)\exp(ik_y y)$. The wavefunction $\Psi_j(x)$ in the three different regions $x < 0$, $0 < x < D$ and $x > D$ are written as

$$\begin{aligned}\Psi_{\rm I}(x) &= e^{ik_x x} + re^{-ik_x x},\\ \Psi_{\rm II}(x) &= ae^{iq_x x} + be^{-iq_x x},\\ \Psi_{\rm III}(x) &= te^{ik_x x},\end{aligned} \tag{4}$$

where r, a, b and t are the amplitudes of the normal reflections and transmission in the left electrodes, the central region and the right electrodes, respectively. Using the continuity conditions at $x = 0$ and $x = D$, we obtain

$$L_1\begin{pmatrix}1\\ r\end{pmatrix} = R_1\begin{pmatrix}a\\ b\end{pmatrix},\quad L_2\begin{pmatrix}a\\ b\end{pmatrix} = R_2\begin{pmatrix}t\\ 0\end{pmatrix},$$

where

$$L_1 = \begin{pmatrix}1 & 1\\ ik_x & -ik_x\end{pmatrix},\ L_2 = \begin{pmatrix}e^{iq_x D} & e^{-iq_x D}\\ iq_x e^{iq_x D} & -iq_x e^{-iq_x D}\end{pmatrix},$$
$$R_1 = \begin{pmatrix}1 & 1\\ iq_x & -iq_x\end{pmatrix},\ R_2 = \begin{pmatrix}e^{ik_x D} & e^{-ik_x D}\\ ik_x e^{ik_x D} & -ik_x e^{-ik_x D}\end{pmatrix},$$

then we can deduce

$$\begin{pmatrix}f\\ g\end{pmatrix} = \begin{pmatrix}\frac{1}{t}\\ \frac{r}{t}\end{pmatrix} = L_1^{-1}R_1L_2^{-1}R_2\begin{pmatrix}1\\ 0\end{pmatrix}$$

and obtain the transmission probability $T = 1/|f|^2$. The wavevectors k_x and q_x can be written as

$$k_x = \sqrt{\frac{E - E_{\rm c}}{(\alpha + (\gamma^2/E_{\rm g}^0)) + \beta\tan^2\theta_0}},\quad k_y = k_x\tan\theta_0,$$
$$q_x = \sqrt{\frac{1}{\alpha + \frac{\gamma^2}{E_{\rm g}}}\left(\frac{E - E_{\rm c}}{1 + \beta\tan^2\theta_0/(\alpha + \frac{\gamma^2}{E_{\rm g}^0})} + V_z\right)}.$$

It is obvious that $E_{\rm g} \geq 0$, i.e., $V_z \leq E_{\rm g}^0/2$, where $q_x \geq 0$, $E_{\rm g}^0 = E_{\rm c} - E_{\rm v}$, $E_{\rm g} = E_{\rm c} - E_{\rm v} - 2V_z$, and E is the incident energy. The corresponding wave functions and the transmission probability along the Γ–Y direction can be obtained by repeating a similar procedure.

The critical angle along the Γ–X direction is

$$\theta_{0{\rm c}}^{(x)} = \arctan\left(\sqrt{\frac{E - E_{\rm c} + V_z}{-V_z}\,\frac{\alpha + (\gamma^2/E_{\rm g}^0)}{\beta}}\right). \tag{5}$$

The critical angle along the Γ–Y direction is

$$\theta_{0{\rm c}}^{(y)} = \arctan\left[\left(\frac{E - E_{\rm c}}{E - E_{\rm c} + V_z} - \frac{\alpha + (\gamma^2/E_{\rm g}^0)}{\alpha + (\gamma^2/E_{\rm g})}\right)^{-1/2}\cdot\left(\frac{\beta}{\alpha + (\gamma^2/E_{\rm g}^0)}\right)^{1/2}\right]. \tag{6}$$

When $\theta_0 > \theta_{0{\rm c}}$, all electron beams are reflected at the interface of junction, which means that the longitudinal wave vector in region II becomes imaginary. Based on the obtained results for the transmission probabilities T, one can find the two-terminal Landauer conductance G for the finite structure. Within a linear regime on bias voltage at very low temperatures, the conductance is given by $G(E_{\rm F}) = G_0(E_{\rm F})\int_{-\pi/2}^{\pi/2} T\cos\theta_0 d\theta_0$ with $G_0 = ge^2E_{\rm F}L/(h^2\upsilon_{\rm F})$ and L the length of the slab in the transverse direction. Here g equals 4 due to the twofold spin and valley degeneracy. We define $\eta = (G_x - G_y)/(G_x + G_y)$, where G_x (G_y) is the conductance for transport along the Γ–X (Γ–Y) direction.

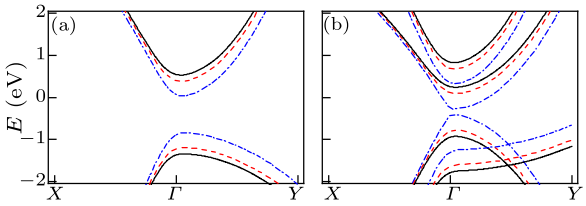

Fig. 2. The energy dispersions with several representative V_z for (a) monolayer phosphorene and (b) bilayer phosphorene. The black, red dashed and blue dot-dashed lines are for $V_z = 0$ eV, 0.15 eV and 0.5 eV, respectively.

Figures 2(a) and 2(b) show the band dispersion of monolayer and bilayer BP along the armchair Γ–X and zigzag Γ–Y directions with an external electric field, where the strong anisotropy of the spectrum is evident. The energy gap $E_{\rm g}^0$ is 1.838 eV for monolayer BP and 1.126 eV for bilayer BP in the absence of the electric field. In the presence of an external electric field, the valence band and conduction band shift in different directions close to the band gap center. This causes a decrease of the band gap with increasing the electric field. The degeneracies of bands have been removed slightly due to the spin orbit coupling (SOC) in comparison with the case of zero SOC coupling except for the time-reversal-invariant momenta which are at

least doubly degenerate according to the Kramers theorem. The gap of phosphorene is located at the Γ point which is a time-reversal-invariant momenta. At this point, the spin-up and spin-down valence and conduction bands are degenerate and the change in the gap due to the SOC is very small as compared to the bulk gap. Therefore, when the bulk gap is modified by an external electric field, we can safely use the spinless Hamiltonian demonstrating the general trend in changes of the gap. Pristine phosphorene as a trivial insulator when the intrinsic SOC effect is included preserves the time-reversal symmetry and can exhibit a quantum spin Hall phase when its electronic properties are influenced by electric field. After a critical electric field, a direct band touching occurs, which is characterized by a topological insulator phase. However, further increase of electric field leads to a metal phase, and because the topological nature does not change, the system may fall into the topological metal phase.

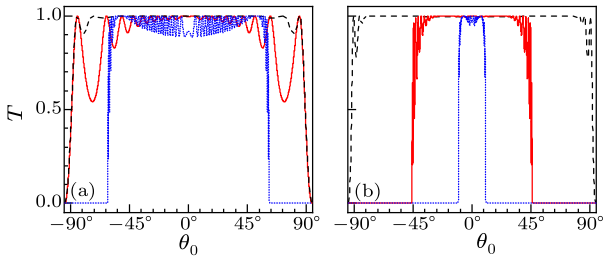

Fig. 3. Transmission probability as a function of the incident angle for (a) monolayer phosphorene and (b) bilayer phosphorene. The incident energy $E = 1\,\text{eV}$. The black dashed line, red solid line and blue short dotted line are for the transmission along k_x direction with $V_z = 0.15\,\text{eV}$, k_y direction with $V_z = 0.15\,\text{eV}$, and k_y direction with $V_z = 0.5\,\text{eV}$.

Figure 3 shows the dependence of the transmission of monolayer and bilayer BP on the incident angle for the fixed incident energy $E = 1\,\text{eV}$ and the bias potential $V_z = 0.15\,\text{eV}$ along the Γ–X (the black dashed line) and Γ–Y directions (the red solid line), $V_z = 0.5\,\text{eV}$ along the Γ–Y direction (the blue short dotted line). The transmission decreases rapidly and then is forbidden when the incident angle exceeds a critical value, where the wavevector q_x in region Ⅱ becomes imaginary, indicating the appearance of evanescent modes. In the presence of an electric field, $\theta_{0c}^{(x)}$ is still always $\pi/2$ when $V_z < E_g^0/2$, while $\theta_{0c}^{(y)}$ decreases with increasing the electric field. The critical angle is different for transport along different directions as the different effective masses along Γ–X and Γ–Y directions. The value of $\theta_{0c}^{(x)}$ is always larger than $\theta_{0c}^{(y)}$ for the fixed incident energy and electric field intensity, which means that the momentum-filtering feature along the Γ–Y direction is more obvious. As the number of layers increases, $\theta_{0c}^{(y)}$ of bilayer phosphorene is smaller than that of monolayer phosphorene for the fixed incident energy and electric field intensity, which is obtained from Eq. (6).

Figures 4(a)–4(d) show the dependence of the transmission of monolayer and bilayer phosphorene on the bias potential V_z for a fixed incident angle $\theta_0 = \pi/4$ and two different incident energies $E = 1\,\text{eV}$ (the black solid line) and $E = 0.8\,\text{eV}$ (the red dashed line) along the Γ–X and Γ–Y directions, respectively. One can see clearly that a sufficiently high electric field could switch off the transport. The critical bias potential along the Γ–X direction is $V_{zc}^{(x)} = E_g^0/2$. It is easily obtained that $V_{zc}^{(x)}$ is 0.919 eV for the monolayer phosphorene and 0.563 eV for the bilayer phosphorene. The critical bias along the Γ–Y direction is $V_{zc}^{(y)} = ((\alpha + \frac{\gamma^2}{E_g})/(\alpha + \frac{\gamma^2}{E_g^0} + \beta\tan^2\theta_0) - 1)(E - E_c)$. When the incident angle $\theta_0 = \pi/4$, there is $V_{zc}^{(y)} = ((\alpha + \frac{\gamma^2}{E_g})/(\alpha + \frac{\gamma^2}{E_g^0} + \beta) - 1)(E - E_c)$. Because $(\alpha + \frac{\gamma^2}{E_g})/(\alpha + \frac{\gamma^2}{E_g^0} + \beta) - 1 < 0$, $V_{zc}^{(y)}$ decreases with increasing the incident energy E. For a fixed incident energy $E = 1\,\text{eV}$, the transmission of monolayer (bilayer) phosphorene along the Γ–Y direction is switched off when the bias potential $V_z \approx 0.57\,\text{eV}$ (0.14 eV). For a fixed incident angle and incident energy, switching off the transmission on bilayer phosphorene only needs an electric field intensity smaller than that on monolayer phosphorene, and for the same number of layers of phosphorene, switching off the transmission along the Γ–X direction compared to that along Γ–Y direction needs a higher electric field intensity, which reflects distinct anisotropic behavior of the phosphorene.

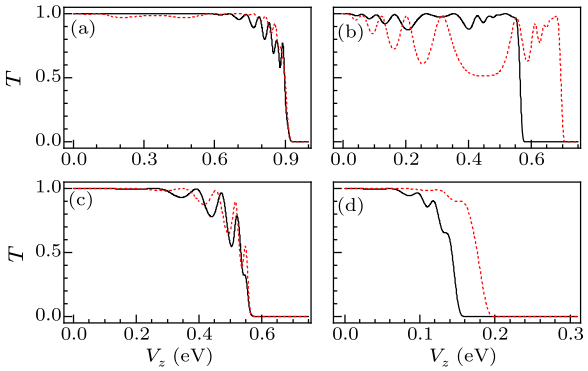

Fig. 4. The transmission probability as a function of V_z along (a) k_x and (b) k_y directions for monolayer phosphorene, while (c) k_x and (d) k_y directions for bilayer phosphorene. The incident angle is fixed at $\theta_0 = \pi/4$. The black solid and red dashed lines are for the incident energy $E = 1\,\text{eV}$ and 0.8 eV, respectively.

To discuss the anisotropic behavior of the conductance, we plot the conductance versus the incident energy for transport through an electric field region with the bias potential $V_z = 0.15\,\text{eV}$ along the Γ–X direction (the black solid line) and the Γ–Y direction (the red dashed line) for the monolayer and bilayer phosphorene in Figs. 5(a) and 5(b), respectively. It is easily seen that the critical incident energy for switching on the transport along the Γ–X direction is the same as that along the Γ–Y direction for a fixed electric field intensity. The zero conductance at low Fermi energy corresponds to the transmission gap shown in Figs. 3 and 4. The critical incident energy is $E = E_c$, which means that the critical incident energy decreases as the number of layers increases. Note that

the conductances for the two transport directions are distinct, and the conductance along the Γ–X direction is larger than that along the Γ–Y direction for the fixed incident energy and electric field intensity. The conductances along both Γ–X and Γ–Y directions exhibit slightly oscillating behaviors. There is a maximum value at the incident energy $E = 0.6\,\text{eV}$ for the conductance along Γ–Y direction (see red dashed line in Fig. 5(b)), thus the difference between the conductances along the Γ–X and Γ–Y directions becomes smaller. This feature is caused by the structure in the transmission discussed above.

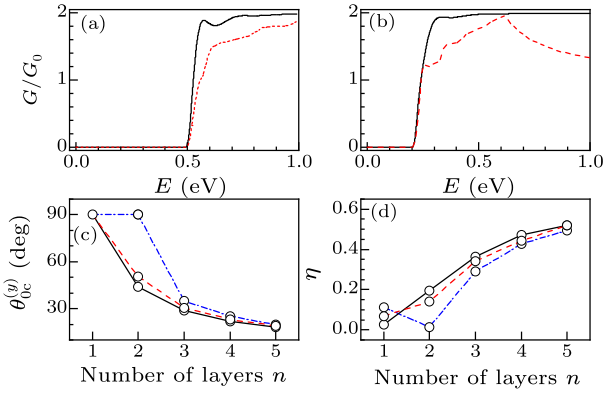

Fig. 5. Conductance as a function of the incident energy for (a) monolayer phosphorene and (b) bilayer phosphorene. The bias potential is $V_z = 0.15\,\text{eV}$. The black and the red dashed lines are for transport along the Γ–X and Γ–Y directions, respectively. (c) The critical angle along the Γ–Y directions and (d) η versus the number of layers for a critical bias potential $V_z = 0.15\,\text{eV}$ and three different incident energies $E = 1\,\text{eV}$ (the black solid line), 0.8 eV (the red dashed line) and 0.6 eV (the blue dot-dashed line), respectively.

Figures 5(c) and 5(d) show the dependence of the critical angle $\theta_{0c}^{(y)}$ and η on the number of layers for a bias potential $V_z = 0.15\,\text{eV}$ and three different incident energies $E = 1\,\text{eV}$ (the black solid line), 0.8 eV (the red dashed line) and 0.6 eV (the blue dot-dashed line), respectively. The value of $\theta_{0c}^{(y)}$ decreases as the number of layers increases for a fixed incident energy, and as the incident energy increases for the fixed number of layers, which can be obtained from Eq. (6). The value of η increases generally as the number of layers increases. For monolayer phosphorene, the smaller the incident energy is, the larger the anisotropy of the conductance is. However, when the number of layers is 2, the smaller the incident energy is, the smaller the anisotropy of the conductance is, which are consistent with the results in Figs. 5(a) and 5(b).

In summary, we have theoretically investigated quantum transport of electron through an external perpendicular electric field region on monolayer and multilayer phosphorene along the Γ–X and Γ–Y directions. Generally, the transmission probability for transport through the electric field region declines sharply and then is blocked when the incident angle exceeds a critical value for a fixed incident energy. The critical value $\theta_{0c}^{(x)}$ along the Γ–X direction is larger than that along the Γ–Y direction, which shows strong anisotropic behavior. The critical angle along the Γ–Y direction decreases as the number of layers or incident energy increases. It is interesting to note that the anisotropy of the conductance can be tuned by the electric field intensity and the number of layers. These results provide an efficient way to control the transport of phosphorene-based microstructures.

References

[1] Novoselov K S, Geim A K, Morozov S V, Jiang D, Katsnelson M I, Grigorieva I V, Dubonos S V and Firsov A A 2005 *Nature* **438** 197
[2] Novoselov K S, Geim A K, Morozov S V, Jiang D, Zhang Y, Dubonos S V, Grigorieva I V and Firsov A A 2004 *Science* **306** 666
[3] Han C Q, Yao M Y, Bai X X, Miao L, Zhu F, Guan D D, Wang S, Gao C L, Liu C, Qian D, Liu Y and Jia J 2014 *Phys. Rev. B* **90** 085101
[4] Lu W, Nan H, Hong J, Chen Y, Zhu C, Liang Z, Ma X, Ni Z, Jin C and Zhang Z 2014 *Nano Res.* **7** 853
[5] Brown A and Rundqvist S 1965 *Acta Crystallogr.* **19** 684
[6] Slater J C, Koster G F and Wood J H 1962 *Phys. Rev.* **126** 1307
[7] Cartz L, Srinivasa S R, Riedner R J, Jorgensen J D and Worlton T G J 1979 *Chem. Phys.* **71** 49010
[8] Ling X, Wang H, Huang S, Xia F and Dresselhaus M S 2015 *Proc. Natl. Acad. Sci. USA* **112** 4523
[9] Maity A, Singh A, Sen P et al 2016 *Phys. Rev. B* **94** 075422
[10] Rodin A S, Carvalho A and Castro Neto A H 2014 *Phys. Rev. Lett.* **112** 176801
[11] Cai K, Liu L, Shi J and Qin Q H 2017 *Mater. Des.* **121** 406
[12] Li X J, Yu J H, Luo K, Wu Z H and Yang W 2018 *Nanotechnology* **29** 174001
[13] Liu H, Du Y, Deng Y and Ye P D 2015 *Chem. Soc. Rev.* **44** 2732
[14] Churchill H O and Jarillo-Herrero P 2014 *Nat. Nanotechnol.* **9** 330
[15] Reich E S 2014 *Nature* **506** 19
[16] Castellanos-Gomez A, Vicarelli L, Prada E, Isl, J O, Narasimha-Acharya K L, Blanter S I, Groenendijk D J, Buscema M, Steele G A, Alvarez J V, Zandbergen H W, Palacios J J and van der Zant H S J 2014 *2D Mater.* **1** 025001
[17] Buscema M, Groenendijk D J, Blanter S I, Steele G A, van der Zant H S J and Castellanos-Gomez A 2014 *Nano Lett.* **14** 3347
[18] Long M, Gao A, Wang P, Xia H, Ott C, Pan C, Fu Y, Liu E, Chen X, Lu W, Nilges T, Xu J, Wang X, Hu W and Miao F 2017 *Sci. Adv.* **3** e1700589
[19] Li L, Yu Y, Ye G J, Ge Q, Ou X, Wu H, Feng D, Chen X H and Zhang Y 2014 *Nat. Nanotechnol.* **9** 372
[20] Liu H, Neal A T, Zhu Z, Luo Z, Xu X, Tománek D and Ye P D 2014 *ACS Nano* **8** 4033
[21] Fei R and Yang L 2014 *Nano Lett.* **14** 2884
[22] Hu S, Xiang J, Lv M, Zhang J, Zhao H, Li C, Chen G F, Wang W H and Sun P J 2018 *Phys. Rev. B* **97** 045209
[23] Wang X, Jones A M, Seyler K L, Tran V, Jia Y, Zhao H, Wang H, Yang L, Xu X and Xia F 2015 *Nat. Nanotechnol.* **10** 517
[24] Qin Z P, Hai T, Xie G Q, Ma J G, Yuan P, Qian L J, Li L, Zhao L M and Shen D Y 2018 *Opt. Express* **26** 8224
[25] Elahi M, Khalij K, Tabatabaei S M, Pourfath M and Asgari R 2015 *Phys. Rev. B* **91** 115412
[26] Cheng F and Yuan Y 2017 *AIP Adv.* **7** 075310
[27] Ezawa M 2014 *New J. Phys.* **16** 115004
[28] Rudenko A N, Yuan S J and Katsnelson M I 2015 *Phys. Rev. B* **92** 085419
[29] Liu Y P, Qiu Z Z, Carvalho A, Bao Y, Xu H, Tan S J R, Liu W, Castro Neto A H, Loh K P and Lu J 2017 *Nano Lett.* **17** 1970
[30] Cheng F and He B 2016 *Chin. Phys. Lett.* **33** 057301